Cite this: DOI: 10.1039/c0xx00000x

www.rsc.org/xxxxxx

ARTICLE TYPE

Development and applications of the LFDFT: the non-empirical account of ligand field and the simulation of the f - d transitions by Density Functional Theory †

Harry Ramanantoanina[a]*, Mohammed Sahnoun[b], Andrea Barbiero[a], Marilena Ferbinteanu[c] and Fanica Cimpoesu[d]*

Received (in XXX, XXX) Xth XXXXXXXXX 20XX, Accepted Xth XXXXXXXXX 20XX

DOI: 10.1039/b000000x

The Ligand Field Density Functional Theory (LFDFT) is a methodology consisting in non-standard handling of DFT calculation and post-computation analysis, emulating the ligand field parameters, in a non-empirical way. Recently, the procedure was extended for two-open-shell systems, with relevance for inter-shell transitions in lanthanides, of utmost importance in understanding the optical and magnetic properties of rare-earth materials. Here, we expand the model to the account of intensities of $f \rightarrow d$ transitions, enabling the simulation of spectral profiles. We focus on Eu^{2+} based systems: this lanthanide ion undergoes many dipole allowed transitions from the initial $4f^7$ ($^8S_{7/2}$) state to the final $4f^65d^1$ ones, considering the free ion and doped materials. The relativistic calculations showed a good agreement with experimental data for gaseous Eu^{2+} ion, producing reliable Slater-Condon and spin-orbit coupling parameters. The Eu^{2+} ions doped fluorite-type lattices, CaF_2: Eu^{2+} and $SrCl_2$: Eu^{2+}, in sites with octahedral symmetry are studied in detail. The related Slater-Condon and spin-orbit coupling parameters from the doped materials are compared to the free ion, revealing small changes for the $4f$ shell side and relatively important shifts for those accounting the $5d$ shell. The Ligand Field scheme, in Wybourne parameterization, shows a good agreement with the phenomenological interpretation of the experiment. The non-empirical computed parameters are used to calculate the energy and intensity of the $4f^7$ - $4f^65d^1$ transitions, rendering a realistic convoluted spectrum.

Dedicated to Professor Claude Daul and Professor Werner Urland in the celebration of their seventieth and seventy-first anniversaries.

Introduction

The concept of ligand field, very fruitful in the effective account of bonding and properties in coordination chemistry is equivalent to the crystal field theory in condensed matter science. Both terminologies refer to the same phenomenological model, operated with adjustable parameters.

Born more than eighty years ago, from the work of H. Bethe [1] and J. H. van Vleck [2] it still keeps the position of the most transparent way to account optical and magnetic properties of metal-ion based systems (lattices or molecular complexes). As long as quantum chemical methods can compute reliable energy level schemes, the subsequent ligand field analysis of the raw results is the way to illuminate in depth the underlying mechanism. [3-5] *Stricto sensu*, the ligand field refers to effective one-electron parameters accounting the effect of the environment on a metal ion, but the complete frame includes the inter-electron effects, describing the electronic correlation in the active space of d^n or f^n configurations, and also the spin-orbit coupling, namely the relativistic effects. Besides the standard theory, one must note the paradigm shift due to C. E. Schäffer and C. K. Jørgensen, who revisited the ligand field theory to ensure more chemical insight within their Angular Overlap Model (AOM), initially devoted to the d-type transition metal systems. [6] W. Urland pioneered this model for the f-type ligand field, in lanthanide compounds, with convincing applications in spectroscopy and magnetism. [7]

About two decades ago, given the important growth of computational techniques, the demand for a predictive theory compatible with the classical formalism of the ligand field theory emerged. Particularly, this is not a trivial task in the frame of Density Functional Theory (DFT), limited to non-degenerate ground states, while ligand field concerns the full multiplets originating from d^n or f^n configurations. In the consistent solving of this problem, C. Daul *erat primus*. He and co-workers (noticing the contribution of M. Atanasov) designed a pioneering approach by non-routine handling of DFT numeric experiments, to extract ligand field parameters, in a post-computational algorithm named LFDFT. [8-10] The procedure treats explicitly the near degeneracy correlation within the model space of the Kohn-Sham orbitals possessing dominant d and f characters.

Cite this: DOI: 10.1039/c0xx00000x

www.rsc.org/xxxxxx

ARTICLE TYPE

Table 1 Total number of generated Slater-determinants corresponding to the $4f^n$ and $4f^{n-1}5d^1$ electron configurations of lanthanide ions having n valence electrons.

n	1	2	3	4	5	6	7	8	9	10	11	12	13	14
$N(4f^n)$	14	91	364	1001	2002	3003	3432	3003	2002	1001	364	91	14	1
$N(4f^{n-1}5d^1)$	10	140	910	3640	10010	20020	30030	34320	30030	20020	10010	3640	910	140
$\sum^a$	24	231	1274	4641	12012	23023	33462	37323	32032	21021	10374	3731	924	141

[a] $\sum$ represents the cumulative sum of $N(4f^n)$ and $N(4f^{n-1}5d^1)$.

In LFDFT, the basic start is a DFT calculation performed in average of configuration (AOC) conditions. Namely, for a given d^n (or f^n) configuration of the metal ion in the complex, the occupation of five (respective seven) Kohn-Sham orbitals carrying main d (or f) character is fixed to the general fractional n/5 (respective n/7) numbers. This corresponds to the barycentre conceived in formal ligand field theories. Subsequently, with the converged AOC orbitals, series of numeric experiments are done, producing the configurations related to the distribution of n electrons in the five (or seven) orbitals identified as the ligand field sequence (this time with corresponding integer populations). These determinant configurations are not real states, but useful computational experiments, able to render ligand field parameters. The situation is somewhat similar to broken symmetry treatments, [11-14] where the spin polarized configurations cannot be claimed as physical states, but artificial constructions relevant for the emulation of the exchange coupling parameters. [15] Then, the LFDFT run of different configurations based on AOC orbitals yields ligand field parameters, altogether with inter-electron Coulomb and exchange effective integrals. Thus, the Slater-Determinants are used as basis in the computational model. In the advanced background of the theory, a canonical number of configurations needed to reproduce the desired parameters can be defined as function of the symmetry of the problem (Slater-Determinant wavefunctions of spin-orbitals weighted by symmetry coefficients). [10] In practice, the full set of configurations can be generated, performing the least square fit relating the computed energy expectation values against the ligand field model formulas. The obtained parameters are further used in setting configuration interaction (CI) matrices, in the spirit of the ligand field formalism, sustained in a non-empirical manner. Therefore C. Daul *et al.* have realized the *parameter-free* ligand field theory, which became a valuable tool for any consideration of multiplet states in DFT.

We recognize herein the impact of the LFDFT in solving various electronic structure problems. This computational gadget has revolutionized many field of chemical science being routinely applied in theoretical investigations [16-20] as well as experimental works. [21,22]

A priori, LFDFT has determined the multiplet energy levels within an accuracy of few hundred wavenumbers. [23] The model has given satisfactory results for the molecular properties arising from single-open-shell system, such as Zero Field Splitting (ZFS), [24,25] magnetic exchange coupling, [26-29] Zeeman interaction, [30] hyper-fine splitting, [30] shielding constants, [31,32], d - d and f - f transitions, [10,17,33,34]

Recently, the LFDFT algorithm has been updated to handle the electronic structure of two-open-shell system as it is important in the understanding of the optical manifestation of lanthanide phosphors. [35,36] Lanthanide compounds are agents in light-emitting diodes (LEDs) technology, used in domestic lighting. [37] In the case of two-open-shell inter-configuration of f and d electrons, the size of the ligand field CI matrices is collected in Table 1, calculated with following combinatorial formulas:

$$N(4f^n) = \binom{14}{n}, \qquad (1)$$

$$N(4f^{n-1}5d^1) = \binom{14}{n-1} \cdot \binom{10}{1}, \qquad (2)$$

as function of the number of active electrons (n). We can confine to a single f - d orbital promotion, since the energy of two and further electron processes is too high. It is seen from Table 1 that the size of the CI matrices increases drastically, for some cases (n = 7 or 8) a parallelized algorithm having been required to achieve calculations.

In this paper we present new development and applications of the LFDFT algorithm, previously validated for the two-open-shell $4f^1 5d^1$ electronic structure of Pr^{3+}. [35,38-40] A special attention will be paid to Eu^{2+} systems, *i.e.* for n = 7 (Table 1) taking as examples divalent europium doped in fluorite-type lattices CaF_2 and $SrCl_2$, comparing the first principles results with the available experimental data. [41,42]

Methodology

The two-open-shell ligand field based CI Hamiltonian in eqn. 3 combines quantum effects due to the inter-electron repulsion and exchange (H_{EE}), the spin-orbit coupling (H_{SO}) and the ligand field effective one-electron (H_{LF}): [35]

$$H = H_0 + H_{EE} + H_{SO} + H_{LF}\,, \qquad (3)$$

where, H_0 is a diagonal matrix, which gathers contributions of zeroth order interactions, such as the kinetic energy background and the nuclear-electron attraction of the AOC configuration:

$$H_0 = -\frac{\hbar^2}{2m}\sum_i \nabla_i^2 - \sum_i \frac{Ze^2}{r_i}\,. \qquad (4)$$

This term acts only on the diagonal of the full ligand field CI matrix:

$$H_0 = \begin{pmatrix} I_{N(4f^n)}.0 & (0) \\ (0) & I_{N(4f^{n-1}5d^1)}.\Delta(fd) \end{pmatrix}, \qquad (5)$$

where, I_N is an identity matrix of dimension N (see Table 1) and $\Delta(fd)$ is the gap parameter, which determines the energy difference between the barycentre of the multiplet levels of the excited $4f^{n-1}5d^1$ and the those of the ground $4f^n$ electron configuration. Therefore, in further consideration, the H_{EE}, H_{SO} and H_{LF} matrices are simply traceless blocks, their possible diagonal elements already engulfed in $\Delta(fd)$.

The matrix elements of H_{EE} are constructed from the two-electron integrals:

$$\langle \psi_a\psi_b | H_{EE} | \psi_c\psi_d \rangle = \int \psi_a^*(r_1)\psi_b^*(r_2)\frac{1}{r_{12}}\psi_c(r_1)\psi_d(r_2)dr_1dr_2\,, \qquad (6)$$

where, ψ denotes the atomic orbital wavefunctions:

$$\psi(r) = R_{nl}(r)Y_{lm}(\theta,\phi)\,, \qquad (7)$$

R_{nl} is the radial wavefunction of the atomic shell and Y_{lm} is the spherical harmonic component. It is a basic assumption of ligand field frame that the two-electron part can be accounted practically like in the free atom. [35]

Within mathematical operations, eqn. 6 is reducible in product of two integrals of angular and radial components. Once the angular part explicitly resolved, the whole variety of eqn. 6 integrals can be represented by few radial Slater-Condon parameters, F_k (eqn. 8 and 9) and G_k (eqn. 10), with intra- or inter-shell nature. In the two-open-shell problem of 4*f* and 5*d* electrons, one obtains:

$$F_k(ff) = \int_0^\infty\int_0^\infty \frac{r_<^k}{r_>^{k+1}} R_{4f}^2(r_1)R_{4f}^2(r_2)r_1^2r_2^2dr_1dr_2\,, \qquad (8)$$

$$F_k(fd) = \int_0^\infty\int_0^\infty \frac{r_<^k}{r_>^{k+1}} R_{4f}^2(r_1)R_{5d}^2(r_2)r_1^2r_2^2dr_1dr_2\,, \qquad (9)$$

$$G_k(fd) = \int_0^\infty\int_0^\infty \frac{r_<^k}{r_>^{k+1}} R_{4f}(r_1)R_{5d}(r_2)R_{5d}(r_1)R_{4f}(r_2)r_1^2r_2^2dr_1dr_2\,. \qquad (10)$$

The matrix elements of H_{SO} express the spin-orbit structure of the electronic multiplets. The formulation of H_{SO} has been the subject of numerous investigations [3,43-45] where its matrix elements have been reasonably well approximated in atomic-like integrals:

$$\langle nlsm_lm_s | H_{SO} | nls'm'_l m'_s \rangle = \zeta_{nl}\langle lsm_lm_s | \hat{l}.\hat{s} | ls'm'_l m'_s \rangle\,, \qquad (11)$$

where, ζ_{nl} is the effective one-electron spin-orbit coupling constants for one electron in a *nl* atomic shell. It can be analytically evaluated using the radial wavefunction R_{nl} of atomic shell:

$$\zeta_{nl} = \frac{Ze^2\hbar^2}{8\pi\varepsilon_0 m_0^2c^2}\langle R_{nl} | \frac{1}{r^3} | R_{nl} \rangle\,. \qquad (12)$$

The matrix elements of H_{LF} play the role of the chemical environment of the lanthanide ion. The general formulation of the ligand field potential follows Wybourne: [46]

$$\langle l_a m_{la} | H_{LF} | l_b m_{lb} \rangle = \sum_{k=0}^{l_a+l_b}\sum_{q=-k}^{k} B_q^k(l_a,l_b)\langle Y_{l_a m_{la}}(\theta,\phi) | C_q^{(k)}(\theta,\phi) | Y_{l_b m_{lb}}(\theta,\phi) \rangle\,, \qquad (13)$$

where, $C_q^{(k)}$ represent the solid spherical harmonic tensor operators (eqn. 11) and B_q^k are the Wybourne-normalized crystal field parameters.

$$C_q^{(k)} = \sqrt{\frac{4\pi}{2k+1}}Y_{kq}\,. \qquad (14)$$

The collection of non-vanishing Wybourne parameters depends to the coordination symmetry of the lanthanide centre, their total number in a two-open-shell *f* - *d* ligand field problem being 64 in case of C_1 point group. [47] Here they cannot be reduced having simple electrostatic origin since the DFT calculation takes into consideration different effects including orbitals overlap and covalence. [35]
Besides the Hamiltonian setting, other specific construction regards the matrix element of the dipole moment operator,

important to the computation of the intensity of transitions:

$$\langle \psi_\mu | \vec{d}_\alpha | \psi_\nu \rangle = \frac{1}{\sqrt{3}} \langle R_{n_\mu l_\mu} | r | R_{n_\nu l_\nu} \rangle \langle Y_{l_\mu m_\mu} | C_\alpha^{(1)} | Y_{l_\nu m_\nu} \rangle , \qquad (15)$$

where, in the right hand side of eqn. 15 the term carrying the radial component is simple overlap integrals while the angular term is proportional with Clebsh-Gordan coefficients. [39] Actually, only the f - d elements are non-vanishing, their mutual mixing by ligand field rendering the intensity, in approximate, but apparently satisfactory manner.

In summary, several series of parameters have to be determined non-empirically in order to perform LFDFT calculation of two-open-shell f and d electrons:

1. $\Delta(fd)$, which represents the energy shift of the multiplets of $4f^{n-1}5d^1$ configuration with respect to those of $4f^n$.
2. $F_k(ff)$, $F_k(fd)$ and $G_k(fd)$, which represent the static electron correlation within the $4f^n$ and $4f^{n-1}5d^1$ configurations.
3. ζ_{nl}, which represents the relativistic spin-orbit interaction in the $4f$ and $5d$ shells.
4. $B_q^k(f,f)$, $B_q^k(d,d)$ and $B_q^k(f,d)$, which describe the interaction due to the presence of the ligands onto the electrons of the metal centre.

The DFT calculations have been carried out by means of the Amsterdam Density Functional (ADF) program package (ADF2013.01). [48-50] We must point out that ADF is one of the few DFT codes having the set of keywords facilitating the AOC calculations and Slater-Determinant emulation, needed by the LFDFT procedure. [35,36] The hybrid B3LYP functional [51] is used to compute the electronic structure and the related optical properties, in line with previous works. [35,36,39] The molecular orbitals are expanded using triple-zeta plus two polarization Slater-type orbital (STO) functions (TZ2P+) for the Eu atom and triple-zeta plus one polarization STO function (TZP) for the Ca, Sr, F and Cl atoms.

The geometrical structures due to the doping of the Eu^{2+} ion into CaF_2 and $SrCl_2$ lattices are approached *via* periodical calculations by means of the VASP program package. [52] The local density approximation (LDA) defined in the VWN [53] and the generalized gradient approximation (GGA) outlined in the PBE [54] are used for exchange–correlation functional. The interaction between valence and core electrons is emulated with the Projected Augmented Wave method. [55,56] External as well as semi-core states are included in the valence. A plane-waves basis set with a cut-off energy of 400 eV is used. Super-cells representing a 2 by 2 by 2 expansion of the unit-cells of CaF_2 and $SrCl_2$ are simulated, which were found to be large enough to lead to render negligible interactions between the periodic images of the Eu^{2+} impurity. 4 k-points were included in each direction of the lattice. The atomic positions were allowed to relax until all forces were smaller than 0.005 eV/Å.

Results and discussion

The determination of $\Delta(fd)$

We must discuss at the very beginning of the calculation of the $\Delta(fd)$ gap, which is important in the problem of two-open-shell systems because it sets the origin of the energy of the two electron configurations, conventionally 0 for the $4f^n$ and $\Delta(fd)$ for the $4f^{n-1}5d^1$. In a first description, we work with the free ion considering the gaseous Eu^{2+} case. Estimating by DFT the energy difference between $4f^65d^1$ and $4f^7$ configurations, we must work under the AOC references. This is because the $\Delta(fd)$ is not the difference between the specific energy levels, but rather a gap of the averaged energy values common for all multiplets of $4f^n$ and $4f^{n-1}5d^1$ kinds.

T. Ziegler *et al.* clarified early that the occupation-averaged configurations, called transition states, carry in DFT the meaning of statistically averaged spectral terms. [57] We prepare the wavefunctions ψ_{4f} and ψ_{5d} by AOC where six and one electrons are evenly distributed in the $4f$ and $5d$ orbitals of Eu^{2+}, respectively (Figure 1). This will generate the reference totally symmetric density, which will be used to compute the DFT energy associated with the series of Slater-determinants. Thus all the Slater-determinant energies are successively computed permuting seven electrons in the $4f$ wavefunction (Figure 1) for the $4f^7$ manifold and permuting six electrons in the $4f$ wavefunction plus one electron in the 5d for the $4f^65d^1$ manifold. The results obtained at the B3LYP level of theory are graphically represented in Figure 2 showing the $\Delta(fd)$ gap. Note that $\Delta(fd)$ can occasionally have a negative value indicating that the ground electron configuration of the lanthanide ion is the $4f^{n-1}5d^1$ instead of the $4f^n$. Such a situation may appear in case of lanthanide Gd^{2+} (n = 8 see Table 1) and La^{2+} (n = 1 see Table 1) ions.

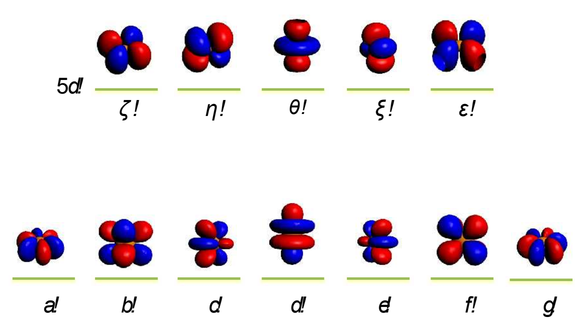

Fig. 1 Representation of the ψ_{4f} and ψ_{5d} orbitals of Eu^{2+} obtained from an AOC calculation of Eu^{2+} within the $4f^65d^1$ electron configuration. The component of the 4f orbitals are listed from left to right according to: $f_{x(x^2-3y^2)}$, f_{xyz}, f_{z^2x}, f_{z^3}, f_{z^2y}, $f_{z(x^2-y^2)}$ and $f_{y(3x^2-y^2)}$, *i.e. a*, *b*, *c*, *d*, *e*, *f* and *g*. The component of the $5d$ orbitals are listed from left to right according to: d_{xy}, d_{xz}, d_{z^2}, d_{yz} and $d_{x^2-y^2}$, *i.e.* ζ, η, θ, ξ and ε.

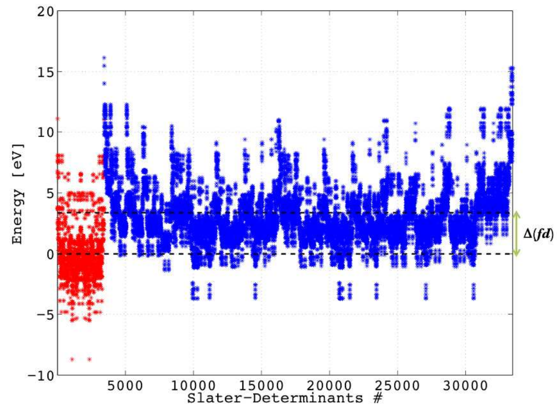

Fig. 2 Representation of the calculated DFT energy values associated with the 3432 Slater-determinants (in red) arising from the $4f^7$ and the 30030 Slater-determinants (in blue) arising from the $4f^6 5d^1$ configurations of Eu^{2+}. The two dashed lines represent the barycentre of the $4f^7$ manifold (set to the zero of energy), and the $4f^6 5d^1$ manifold.

The lowest energies corresponding to the $4f^7$ manifold (Figure 2) are associated to the Slater-determinants:

$$\left|a^+b^+c^+d^+e^+f^+g^+\right| \text{ and } \left|a^-b^-c^-d^-e^-f^-g^-\right|,$$

where, the sign + and - represent the spin of one electron according to up and down, respectively. The highest energies corresponding to the $4f^6 5d^1$ manifold (Figure 2) are associated to the Slater-determinants:

$$\left|c^\pm d^\pm e^+ \theta^+\right| \text{ and } \left|c^\pm d^\pm e^+ \theta^-\right|,$$

where, the sign ± represents a restricted occupation of two electrons in one orbital. The calculated value of the $\Delta(fd)$ parameter is 3.10 eV at the B3LYP level of theory.

The DFT Slater-determinants energies (Figure 2) can provide also information about the two-electron $F_k(ff)$, $F_k(fd)$ and $G_k(fd)$ parameters using Slater's rule [3] and least mean square fit. [10] However, this procedure might undergo uncertainty caused by the important number of linear equations *versus* variables. In case of two-open-shell $4f^7$ and $4f^6 5d^1$ of Eu^{2+} for instance, it returns to solve 33462 linear equations with nine variables leading to some misrepresentations of the parameters. [58] Therefore we calculate the $F_k(ff)$, $F_k(fd)$ and $G_k(fd)$ parameters from the radial wavefunctions R_{nl} of the 4*f* and 5*d* Kohn-Sham orbitals of the lanthanide ions following eqn. 8 - 10, being the subject of the next section.

The calculation of F_k, G_k, and ζ_{nl} parameters

The importance of relativity in the physics of lanthanide elements is not negligible. [59-63] There are different manners dedicated to the implementation of relativistic corrections in DFT. Besides the spin-orbit interaction H_{SO} (eqn. 11), which has itself a relativistic origin; the physics behind the Dirac equation in quantum chemistry is reasonably well characterized by the scalar-relativistic equations. [64] We can perform scalar-relativistic calculations at the zeroth order regular approximation (ZORA) to the Dirac equation [65-69] or the first order relativistic Pauli Hamiltonian [70-74] in DFT. In Figure 3, the solutions of the radial wavefunctions of the 4*f* and 5*d* Kohn-Sham orbitals obtained for gaseous Eu^{2+} ion are graphically represented, where the influence of the relativistic correction is evaluated. A noticeable expansion of the R_{nl} is observed while relativistic corrections are implemented in the computational details (Figure 3), in line with the definition of relativity acting on *f* and *d* orbitals. [64,75] This expansion is severely pronounced for the Pauli-relativistic calculation (Figure 3) because of the explicit account of the Darwin and mass-velocity terms in the master equation. [70-74] The calculated $F_k(ff)$, $F_k(fd)$, $G_k(fd)$ and ζ_{nl} parameters using R_{4f} and R_{5d} (Figure 3) are collected in Table 2. In total there are:

three $F_k(ff)$ parameters: $F_2(ff)$, $F_4(ff)$ and $F_6(ff)$; plus
two $F_k(fd)$ parameters: $F_2(fd)$ and $F_4(fd)$; plus
three $G_k(fd)$ parameters: $G_1(fd)$, $G_3(fd)$ and $G_5(fd)$; plus
two spin-orbit coupling constants: ζ_{4f} and ζ_{5d}. [35]

The parameters in Table 2 are determined from the wavefunctions ψ_{4f} and ψ_{5d} prepared in the same manner as it is done in Figure 1.

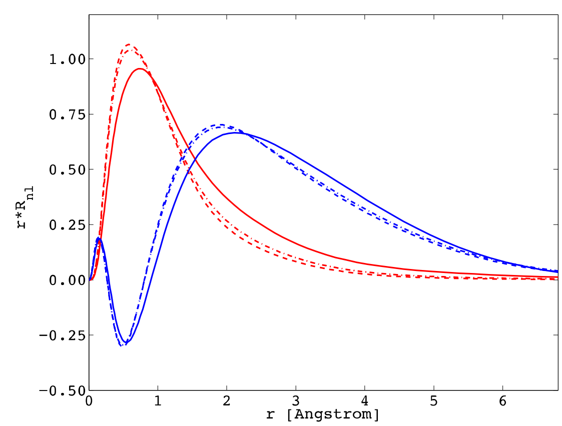

Fig. 3 Representation of the radial wavefunctions R_{nl} corresponding to the 4*f* (in red) and 5*d* (in blue) Kohn-Sham orbitals of gaseous Eu^{2+} ion, obtained at the Pauli-relativistic (solid curve), the ZORA-relativistic (dotted-and-dashed curve) and the non-relativistic (dashed curve) levels of theory.

Table 2 Calculated Slater-Condon parameters and spin-orbit coupling constants (in cm^{-1}) obtained at the non-relativistic (a), the ZORA-relativistic (b) and the Pauli-relativistic (c) levels of theory, corresponding to the two-open-shell $4f^7$ and $4f^6 5d^1$ electron configurations of gaseous Eu^{2+} ion.

	Slater-Condon parameters and spin-orbit coupling constants		
	(a)	(b)	(c)
$F_2(ff)$	500.19	475.60	388.47
$F_4(ff)$	64.66	61.32	49.92
$F_6(ff)$	6.87	6.51	5.30
$F_2(fd)$	245.32	245.36	244.72
$F_4(fd)$	17.86	18.12	18.82
$G_1(fd)$	338.38	369.81	431.92
$G_3(fd)$	29.97	31.66	35.34
$G_5(fd)$	4.70	4.91	5.40
ζ_{4f}	2133.90	1980.90	1246.50
ζ_{5d}	1279.31	1245.93	987.25

Table 3 Calculated multiplet energy levels (calc.) of gaseous Eu^{2+} ion (in cm^{-1}) at non-relativistic (a), ZORA-relativistic (b) and Pauli-relativistic (c) levels of theory, compared with the experimentally known spectral terms (exp.) corresponding to the $4f^7$ electron configuration.

	calc.			exp.[a]
	(a)	(b)	(c)	
$^8S_{7/2}$	0.00	0.00	0.00	0.00
$^6P_{7/2}$	36379.05	34596.14	28854.94	28200.06
$^6P_{5/2}$	37400.88	35526.15	29317.04	28628.54
$^6P_{3/2}$	38339.68	36381.98	29758.39	-[a]
$^6I_{7/2}$	40277.33	38282.44	31591.89	31745.99
$^6I_{9/2}$	40978.41	38917.65	31888.23	31954.21
$^6I_{17/2}$	41370.71	39274.11	32060.93	32073.30
$^6I_{11/2}$	41542.51	39430.07	32135.09	32179.55
$^6I_{15/2}$	41901.08	39756.07	32293.32	32307.78
$^6I_{13/2}$	41881.85	39739.21	32287.83	32314.14

[a] taken from ref. [76] where the energy value of $^6P_{3/2}$ is not known.

Note that the parameters $F_2(ff)$, $F_4(ff)$ and $F_6(ff)$ are acting principally on the single-open-shell $4f^n$ configuration but they are also present in the diagonal block of the $4f^{n-1}5d^1$ interaction matrix. Experimentally known spectral terms of the $4f^7$ configuration of Eu^{2+} concern only the ground state ^8S and the two excited states ^6P and ^6I, [76] although there are 119 levels arising from the multi-electron configuration. [77] The calculated energy values of these ^8S, ^6P and ^6I spectral terms are given in Table 3, obtained using the parameters in Table 2. They are also compared with the available experimental data taken from the framework of the NIST atomic spectra database. [76]

We determine the deviations between the calculated and the experimental spectral terms (Table 3) using eqn. 16. For the three computational methods into consideration, we obtain a maximum deviation of 30.64 %, 24.09 % and 2.41 %, respectively for the non-relativistic, ZORA-relativistic and Pauli-relativistic calculations. On the other hand, we also obtain a minimum deviation of 26.87 %, 20.59 % and 0.04 %. There is an appropriate agreement between the Pauli-relativistic results and the experimental data.

$$\varepsilon[\%] = 100.\frac{|E_{calc} - E_{\exp}|}{E_{\exp}}, \qquad (16)$$

Experimentally known spectral terms of the $4f^6 5d^1$ configuration of Eu^{2+} in [76] assemble some states of octet and sextet spin multiplicity, which in tensor operator techniques represent the direct product: $4f^6\,(^7F) \otimes {}^2D$, giving rise to the following terms: ^8P, ^6P, ^8D, ^6D, ^8F, ^6F, ^8G, ^6G, ^8H and ^6H. Note that the whole manifold of the $4f^6 5d^1$ configuration lets the consideration of 906 spectral terms, including not only the high octet spin multiplicity but also the lower sextet, quartet and doublet, which energies are obtained from the DFT calculation using $F_k(ff)$, $F_k(fd)$, $G_k(fd)$, ζ_{4f} and ζ_{5d} parameters (Table 2) and $\Delta(fd)$ parameter discussed in the previous section.

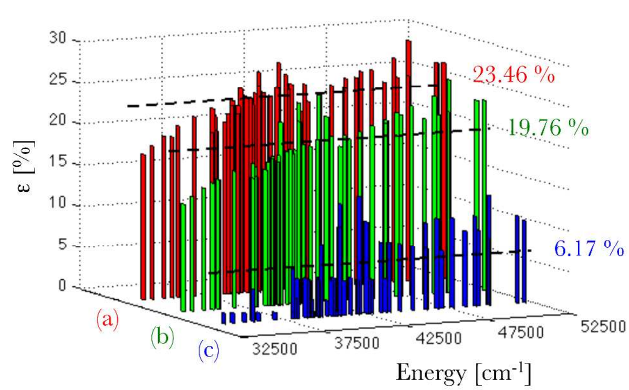

Fig. 4 Representation of the error distribution ε (in %) with respect to the experimental data [76] of the calculated multiplet energy levels corresponding to the $4f^6 5d^1$ configuration of gaseous Eu^{2+} ion at non-relativistic (in red, (a)), ZORA-relativistic (in green, (b)) and Pauli-relativistic (in blue, (c)) levels of theory. The calculated mean deviations with the experimental data are also given.

The calculated deviations ε (eqn. 16) with the experimentally known spectral terms [76] are represented in Figure 4 for the three theoretical methods into consideration. Here also the Pauli-relativistic calculation leads to the best reproduction of the experimental data, its mean deviation represents 6.17 % (Figure 4), which is far smaller if compared to those obtained at non-relativistic and ZORA-relativistic levels of theory.

In this section, the impact of the relativistic correction into the spectroscopy of lanthanide ions is clearly justified; an appropriate description of the radial R_{4f} and R_{5d} wavefunctions is a prerequisite, enabling a good reproduction of the experimental data.

The structural analysis of doped system

The doping of lanthanide ions into solid state materials is nowadays the topic of significant interest due to optical effects. [37] There are several instrumental methods to probe the local structure around the impurity ions in solid state compounds such as nuclear magnetic resonance (NMR), [78] extended X-ray absorption fine structure (EXAFS), [79,80] as well as electron paramagnetic resonance (EPR). [81] However, these methods do not give direct results of the local geometry, offering only data that can be corroborated to it. A clear answer is found in the theoretical side, mimicking the doping of solid state materials by means of band structure methods. In this section we investigate the local structure around the Eu^{2+} impurity, while it is incorporated in the matrices of CaF_2 and $SrCl_2$. The calcium fluoride (CaF_2) and strontium chloride ($SrCl_2$) belong to the cubic Fm-3m space group (N° 225). [41,42] The divalent Eu^{2+} ion enters in the matrices in the site formally occupied by Ca^{2+} and Sr^{2+}. It is then coordinated by eight fluoride and chloride ligands, respectively in the system CaF_2:Eu^{2+} and $SrCl_2$:Eu^{2+}, within O_h point group.

For the pristine CaF_2 and $SrCl_2$ systems (Figure 5), the calculated lattice parameters are given in Table 4 in terms of the DFT functional used in the band structure algorithm. It is found that both GGA and LDA calculations yield different lattice equilibrium constants (Table 4), *i.e* different local relaxations. In terms of direct comparison, we consider the GGA calculation most appropriate to simulate the experimental data although the cells are slightly larger than the experimental.

Table 4 Calculated lattice parameters *a*, *b*, *c* (in Å) and α, β, γ (in °) obtained for CaF_2 and $SrCl_2$ crystallizing in the cubic Fm-3m space group (N° 225), compared with the experimental X-ray diffraction data.

	CaF_2			$SrCl_2$		
	LDA	GGA	exp.^{a}	LDA	GGA	exp.^{b}
a, b, c	5.3342	5.5179	5.4355	6.8088	7.0472	6.965
α, β, γ	90.0	90.0	90.0	90.0	90.0	90.0

^{a} taken from ref. [82]
^{b} taken from ref. [83]

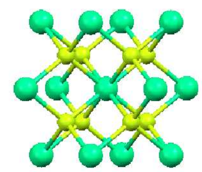

Fig. 5 Representation of the crystal structure of CaF_2 showing the unit-cell (left hand side). The local structure of Eu^{2+} centre embedded in a 2×2×2 unit-cells of CaF_2 (right hand side). Colour code: Ca^{2+} in green, F^- in yellow and Eu^{2+} in violet. For clarity, some Ca^{2+} and F^- ions are represented in wireframe shape.

For the CaF_2:Eu^{2+} and $SrCl_2$:Eu^{2+} systems, we construct super-cells which double the number of the unit-cell of CaF_2 and $SrCl_2$ in the *a*, *b* and *c* directions. The Eu^{2+} ion is placed in the position (0, 0, 0). In these cases, the super-cells are big enough inasmuch as the interactions between two Eu^{2+} ions are minimized. We relax the positions of the atoms fixing the lattice parameters to the theoretical values obtained for the pure systems. This mimics the resistance of the whole lattice against defect induced distortions, in conditions of a lower doping concentration than the actually worked upon 2×2×2 super-cells. The optimized Eu-F and Eu-Cl bond lengths are 2.4732 Å and 3.0774 Å, respectively, which represent an elongation with respect to the Ca-F and Sr-Cl bond lengths obtained for the pure systems: 2.3893 Å and 3.0515 Å. The description of the local structure of doped materials is important in the further evaluation of the ligand field Hamiltonian (eqn. 13), the presence of the impurity in the host materials producing distortions due to difference in ionic radii or electronic structure. We favoured here the band structure algorithms for geometrical purpose although we can certainly conceive a cluster geometry optimization approach, which is already popular in computational chemistry especially while dealing with excited states geometry. [36,39]

The calculation of B_q^k ligand field parameters

In the CaF_2:Eu^{2+} and $SrCl_2$:Eu^{2+} systems, the site symmetry of the Eu^{2+} impurity is O_h and the non-zero Wybourne parameters are:

$$B_0^4(f,f),\ B_4^4(f,f),\ B_{-4}^4(f,f),\ B_0^6(f,f),\ B_4^6(f,f) \text{ and } B_{-4}^6(f,f)$$

for the sub-matrix corresponding to the $\langle f|H_{LF}|f\rangle$ (eqn. 13);

$$B_0^4(d,d),\ B_4^4(d,d) \text{ and } B_{-4}^4(d,d),$$

for the sub-matrix corresponding to the $\langle d|H_{LF}|d\rangle$ (eqn. 13).

The inversion center in the O_h point group allows vanishing of the elements of the sub-matrix $\langle f|H_{LF}|d\rangle$. [47]

The ligand field energy schemes of the 4*f* and the 5*d* orbitals of Eu^{2+} in the $CaF_2:Eu^{2+}$ and $SrCl_2:Eu^{2+}$ systems are calculated taking the cubic clusters $(EuF_8)^{6-}$ and $(EuCl_8)^{6-}$, respectively, having the optimized geometries obtained in the previous section. Point charges are placed at the coordinates of the next neighbouring Ca^{2+} and Sr^{2+} ions which are also seen in ball-and-sticks in the super-cell in Figure 5. These are used in order to mimic the long range interaction of the crystal hosts.

The ligand field energies and wavefunctions are obtained from Kohn-Sham orbitals of restricted DFT calculations within the AOC reference, by placing evenly six electrons in the 4*f* orbitals and one electron in the 5*d*. We early presented the analysis of the ligand field interaction with respect to the change of the DFT functional for the two-open-shell 4*f* and 5*d* problem in Pr^{3+}. [35] It is found that in the 5*d* ligand field, DFT functional does not plays important role, whereas in the 4*f*, the hybrid B3LYP functional is required in order to obtain realistic ligand field parameters. [35] Therefore we use B3LYP for the computation of the electronic structure of Eu^{2+}.

The 4*f* orbitals form the basis of t_{1u}, t_{2u} and a_{2u} irreducible representations (*irreps*) of the O_h point group. The 5*d* orbitals are in the basis of the e_g and the t_{2g} *irreps*. The values of the ligand field B_q^k parameters are determined by linear equation fitting using eqn. 13, knowing the following ratios proper to the octahedral symmetry constraint:

$$B_4^4(l,l) = B_{-4}^4(l,l) = \sqrt{\frac{5}{14}} B_0^4(l,l), \qquad (17)$$

with *l* standing for *d* and *f*, and

$$B_4^6(f,f) = B_{-4}^6(f,f) = -\sqrt{\frac{7}{2}} B_0^6(f,f). \qquad (18)$$

Table 5 Calculated ligand field parameters (calc.) in cm^{-1} obtained for the systems $CaF_2:Eu^{2+}$ and $SrCl_2:Eu^{2+}$, compared with experimental available data (exp.).

	$CaF_2:Eu^{2+}$		$SrCl_2:Eu^{2+}$	
	calc.	exp.[a]	calc.	exp.[b]
$B_0^4(f,f)$	-1765	-2386	-829	-1035
$B_4^4(f,f)$	-1055	-1430	-496	-619
$B_0^6(f,f)$	120	966	208	-761
$B_4^6(f,f)$	-225	-1807	-389	1423
$B_0^4(d,d)$	-34821	-33600	-21086	-21296
$B_4^4(d,d)$	-20810	-20080	-12601	-12727

[a] taken from ref. [41]
[b] taken from ref. [42]

The calculated values of the B_q^k parameters for the $CaF_2:Eu^{2+}$ and $SrCl_2:Eu^{2+}$ systems are presented in Table 5, together with the experimentally deduced ones. For $B_q^k(d,d)$, the theoretical values are in good agreement with the experimental data. [41,42] However for $B_q^k(f,f)$, although the $B_0^4(f,f)$ and *ipso facto* the $B_4^4(f,f)$ (eqn. 17) are also in the magnitude of the experimental data, the $B_0^6(f,f)$ and related parameters (eqn. 18) are slightly underestimated for both $CaF_2:Eu^{2+}$ and $SrCl_2:Eu^{2+}$ systems. This departure between the calculated and the experimental values is reflected primarily the ordering of the 4*f* orbitals splitting. This ordering obtained from computation is for both $CaF_2:Eu^{2+}$ and $SrCl_2:Eu^{2+}$ systems as:

$$t_{1u} < t_{2u} < a_{2u},$$

while it resulted in he swapped sequence:

$$t_{1u} < a_{2u} < t_{2u}$$

for the experimental deduced parameters obtained for the $SrCl_2:Eu^{2+}$ system. [42]

The change in the orbital ordering may be attributed to the impact of the neighbouring cations, where the symmetry adapted linear combination of their virtual orbitals may stabilize the a_{2u} *irrep*. This is not achieved here in the small cluster models of $(EuCl_8)^{6-}$. Nevertheless, a direct comparison between $B_q^k(f,f)$ and $B_q^k(d,d)$ indicates that the effect of the 4*f* parameters will be completely superseded by the 5*d* ones.

AOM analysis of the ligand field interaction

For the sake of more intuitive insight, the B_q^k parameters can be converted to the AOM scheme, [47] reformulating the ligand field matrix in eqn. 13 as follows:

$$\langle 3,m|H_{LF}|3,m'\rangle = \sum_{k=1}^{ligands} \sum_{\lambda=\sigma,\pi} D_{m,\lambda}^{4f}(k) \,.\, D_{m',\lambda}^{4f}(k) \,.\, e_{\lambda,k}(4f), \qquad (19)$$

$$\langle 2,m|H_{LF}|2,m'\rangle = \sum_{k=1}^{ligands} \sum_{\lambda=\sigma,\pi} D_{m,\lambda}^{5d}(k) \,.\, D_{m',\lambda}^{5d}(k) \,.\, e_{\lambda,k}(5d), \qquad (20)$$

where, D^{4f} and D^{5d} are the matrix elements defined in terms of Euler angles (Wigner's Darstellungsmatrizen) [6,7,47] and *k* is the running index for the ligand system. The $e_\lambda \equiv e_\sigma, e_\pi$ parameters have the meaning of perturbation exerted by σ and π sub-components of density cloud of the ligands (or by corresponding overlap effects, in another heuristic formulation).

A general problem in establishing the parametric conversion is the fact that the AOM matrix is not traceless, the sum of the diagonal elements for a homoleptic $[ML_n]$ complex with linearly ligating ligands (isotropic π effects) being $n(e_\sigma + 2e_\pi)$, instead of zero, like in standard ligand field model. In the case of the 4*f* shell, in octahedral symmetry, the situation does not impinge upon the parametric conversion since we have two independent parameters, $B_0^4(f,f)$ and $B_0^6(f,f)$ in the Wybourne scheme (Table 5), *versus* two AOM parameters $e_\sigma(4f)$ and $e_\pi(4f)$, uniquely related to the two relative gaps in the ligand field splitting in O_h symmetry.

The mutual conversion is done by the following formulas:

$$e_\sigma(4f) = -\frac{9}{44}B_0^4(f,f) + \frac{63}{1144}B_0^6(f,f)\,, \quad (21)$$

$$e_\pi(4f) = -\frac{3}{22}B_0^4(f,f) - \frac{189}{1144}B_0^6(f,f), \quad (22)$$

The comparison of computed *versus* experimental fitted Wybourne parameters (Table 5) can be regarded as semi-quantitative in general, with certain apparent mismatches, as is the opposite sign found for the $B_0^6(f,f)$ value in the case of the $SrCl_2:Eu^{2+}$ system. The same sign mismatch in the case of computed *versus* fitted $B_4^6(f,f)$ is not an independent feature, given the mentioned $B_4^6(f,f)/B_0^6(f,f)$ proportionality (eqn. 18). The conversion to AOM parameterization allows a certain assessment of the situation. Thus, the calculated AOM parameters for the $SrCl_2:Eu^{2+}$ system are (in cm^{-1}): $e_\sigma(4f) = 181.02$ and $e_\pi(4f) = 78.68$, while the conversion of reported fitted $B_0^4(f,f)$ and $B_0^6(f,f)$ values [42] yields: $e_\sigma(4f) = 169.79$ and $e_\pi(4f) = 266.86$. One observes that the experimental values lead to the somewhat counterintuitive situation of $e_\pi(4f) > e_\sigma(4f)$ values, resulting then that the numeric experiment may be, in relative sense, a more reliable source, not for absolute values but with respect of the inter-parametric ratios. The fact is that the ligand field parameters on 4*f* shell show small values, in general, being prone to fit uncertainties given the large amount of active parameters. The reference work [42] considered a fit with several empiric terms such as Trees and Marvin corrections, while keeping imposed fixed ratios among the more fundamental Slater-Condon parameters, and therefore the full comparability of computed *versus* fitted parameters is partly hindered, considering that we worked here only with respect of first-principle conceivable leverages: ligand field, Slater-Condon and Spin-Orbit coupling parameters, without other degrees of freedom.

For the 5*d* shell, the single gap between e_g and t_{2g} does not need the two AOM parameters, so that must impose certain conventions, like the $e_\sigma(5d)/e_\pi(5d) = 3$ ratio. [35] However, we do not advance in this direction, since given the good match of the computed and fitted 5*d*-type B_q^k parameters which do not demand the call of AOM as further moderator in the comparative discussion.

The ligand field interaction, besides lifting the degeneracy of the 4*f* and 5*d* orbitals, has also a side effect expanding the radial wavefunctions towards the ligands positions. This is commonly known as nephelauxetic effect, a concept coined by C. K. Jørgensen [84] which is the subject of the next section.

The nephelauxetic effect

The nephelauxetic effect describes the fact that the parameter values of the inter-electron repulsion are usually smaller in complexes than in the corresponding free ions. [84] The word nephelauxetic was created by basic translation of "cloud expansion" from Greek. We can quantitatively analyze the changes in the metal wavefunctions with respect to the presence of ligands, underlying the action of nephelauxetic effect. The 4*f* shell is shielded from the interaction with the chemical environment inasmuch as independently to the ligand type, the reduction of the free ion inter-electron repulsion $F_k(ff)$ parameters are negligible. [47,85] On the other hand, the virtual 5*d* and 6*s* shells are able to interact with the neighbourhood, ensuring therefore the bonding of lanthanide ions. [86-88] We present in Figure 6 the radial wavefunction R_{5d} of Eu^{2+} in the presence of eight fluoride and eight chloride ligands in a cubic arrangement. For comparison purpose, we represent also the radial wavefunction obtained in the gaseous Eu^{2+} free ion (Figure 3). One observes the pronounced expansion of R_{5d} in the series of fluoride and chloride ligands highlighting the overlap of ligands by the orbitals from the lanthanide ion. Due to this effect, as explained in previous instances, in the excited states of $4f^{n-1}5d^1$ lanthanide configuration, the calculated bond lengths are always shorter than that obtained in the ground $4f^n$ configuration. [36,39] Recalling eqn. 9 and 10 we calculate the $F_k(fd)$ and $G_k(fd)$ parameters in the complex, based on radial shapes shown in Figure 6. Compared with Figure 3 one notes that R_{4f} remains almost the same, while R_{5d} were shifted by the nephelauxetic effect (see also ref. [47]).

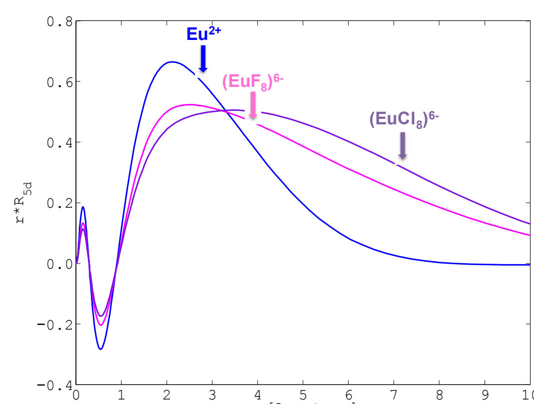

Fig. 6 Representation of R_{5d} of Eu^{2+} in the free ion (in blue), in $(EuF_8)^{6-}$ (in pink) and $(EuCl_8)^{6-}$ (in violet), obtained at the Pauli-relativistic level of theory.

Table 6 Calculated values of the Slater-Condon $F_k(fd)$ and $G_k(fd)$, the spin-orbit coupling ζ_{5d} and the $\Delta(fd)$ gap (in cm^{-1}) obtained for the systems $CaF_2:Eu^{2+}$ and $SrCl_2:Eu^{2+}$; compared with the experimentally deduced values.

	$CaF_2:Eu^{2+}$			$SrCl_2:Eu^{2+}$		
	calc.	β	exp.^{a}	calc.	β	exp.^{b}
$F_2(fd)$	138.42	0.57	133.33	100.56	0.41	117.43
$F_4(fd)$	9.88	0.53	10.25	6.79	0.36	8.54
$G_1(fd)$	232.08	0.54	192.29	160.56	0.37	162.06
$G_3(fd)$	18.22	0.52	17.30	12.31	0.35	14.41
$G_5(fd)$	2.74	0.51	2.72	1.84	0.34	2.26
ζ_{5d}	505.76	0.51	760	371.14	0.38	844
$\Delta(fd)$	18800	-	23500	12400	-	-

^{a,b} The $F^k(fd)$ and $G^k(fd)$ are taken from refs. [41] and [42]. They are converted to the corresponding $F_k(fd)$ and $G_k(fd)$ parameters using the conversion factor in ref. [43]

The results are given in Table 6 together with the calculated spin-orbit coupling constant ζ_{5d} using eqn. 12 and the $\Delta(fd)$ gap. All the parameters (Table 6) are reduced, if compared to the Pauli-relativistic quantities in Table 2. The nephelauxetic ratio β is defined as the fraction made from the inter-electron parameters obtained in the complex and in the free ion, for instance:

$$\beta(F_2(fd)) = \frac{F_2(fd)_{\text{Complex}}}{F_2(fd)_{\text{Free Ion}}}. \qquad (23)$$

The calculated β values for $F_k(fd)$, $G_k(fd)$ and ζ_{5d} are also given in Table 5. We calculate a mean β values of 0.53 and 0.37 for the $CaF_2:Eu^{2+}$ and $SrCl_2:Eu^{2+}$, respectively.

We can obtain the $\Delta(fd)$ gap for the $CaF_2:Eu^{2+}$ system from ref. [41] which we compare with our calculated value (Table 6). Unfortunately the experimental value for the same parameter is not specified for the $SrCl_2:Eu^{2+}$ system. [42] The difference between the calculated $\Delta(fd)$ gap and that obtained in [41] is directly related to the $F_k(ff)$ parameters (Table 2) which is also present in the diagonal elements of the CI matrix of the $4f^65d^1$ configuration of Eu^{2+}. Since the values of our calculated $F_k(ff)$ parameters are larger than that given in ref. [41] our $\Delta(fd)$ is accordingly smaller.

The $4f^7$ - $4f^65d^1$ transitions

The multiplet energy levels corresponding to the $4f^7$ and the $4f^65d^1$ configurations of Eu^{2+} doped into CaF_2 and $SrCl_2$ are given in Figure 7 in the spectral range of 0 - 55000 cm^{-1} (the entire spectral range are given in the Electronic Supplementary Information ESI: Figure S1 and Figure S2). They are computed in the LFDFT algorithm using the non-empirical parameters: $F_k(ff)$ and ζ_{4f} (Table 2); $F_k(fd)$, $G_k(fd)$, ζ_{5d} and $\Delta(fd)$ (Table 6); and B_q^k's parameters (Table 5).

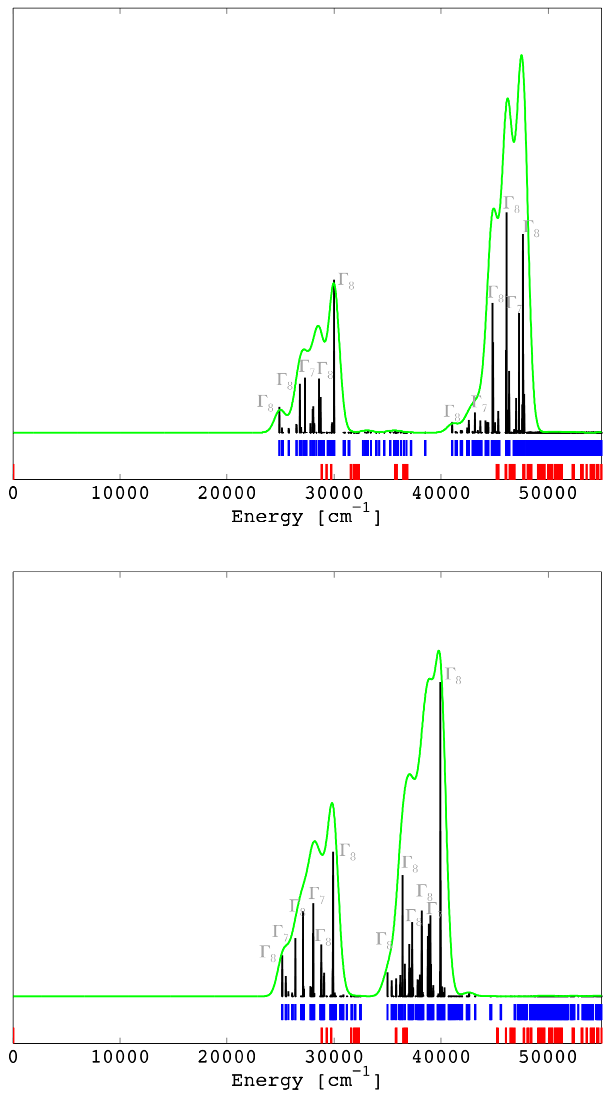

Fig. 7 Calculated multiplet energy levels from the $4f^7$ (in red) and $4f^65d^1$ (in blue) configurations of Eu^{2+} in CaF_2 (up) and $SrCl_2$ (down) together with the intensities of the excitation $4f^7 \rightarrow 4f^65d^1$ transitions, *i.e.* zero phonon lines (in black). The green curve represents a superimposition of a Gaussian band with a width of 500 cm^{-1} on the zero phonon lines.

The transitions from the initial $4f^7$ ($^8S_{7/2}$) state to the final $4f^65d^1$ are electric dipole allowed, where the calculation of the electric dipole transition moments is obtained from eqn. 15. The oscillator strength for the zero phonon lines between the ground state $^8S_{7/2}$ of $4f^7$ and the final states of $4f^65d^1$ are calculated and represented in Figure 7. The most intense transitions are given with respect to the *irreps* of the octahedral double group. In the circumstances of non-degenerate $^8S_{7/2}$ state of the $4f^7$ subsystem, the energies of the $4f^7$ - $4f^65d^1$ transitions are practically the same with the position of $4f^65d^1$ spectral terms. The intensities are computed by corresponding handling of dipole moment represented in the ligand field CI basis, depending all on a single reduced matrix element, ultimately irrelevant as absolute value, if we consider an arbitrary scale of spectral rendering. The zero field splitting, which transform the $^8S_{7/2}$ state of $4f^7$ to $\Gamma_6 + \Gamma_7 + \Gamma_8$ in the actual octahedral symmetry, is in the magnitude of tenths of cm^{-1}. The $4f^65d^1$ transitions are characterized by two dominant bands (Figure 7), in line with the excitation spectrum seen in [41] and [42] for $CaF_2:Eu^{2+}$ and $SrCl_2:Eu^{2+}$. The correspondence between the theoretical results and the excitation spectrum is seen in the ESI where the excitation spectra of $CaF_2:Eu^{2+}$ (Figure S1) and $SrCl_2:Eu^{2+}$ (Figure S2) are reproduced from ref. [41] and [42]

Conclusions

Optical and magnetic effects in lanthanide based compounds are phenomena intimately understood with the help of ligand field theory. In this work, we have drawn important points for a realistic description of the electronic structure and the optical properties of Eu^{2+}-doped CaF_2 and $SrCl_2$ compounds. The treatment of the local distortions due to the presence of the Eu^{2+} impurity in the fluorite structure of CaF_2 and $SrCl_2$ is addressed by periodical band structure calculation. The LFDFT algorithm is used for the calculation of the multiplet energy levels of the $4f^7$ and $4f^65d^1$ electron configurations of Eu^{2+}. The optical $4f^7$ - $4f^65d^1$ transitions are determined, a good qualitative agreement between the non-empirical investigations and the experimental findings being achieved. In particular the convoluted calculated spectrum can be immediately confronted with experimental data, thus showing the usefulness of the approach to experimental scientists. The computational methods and post-computational analyses comprised in the LFDFT algorithm are producing reliable ligand field and related parameters, consolidating the academic insight into the structure-property relationships of rare-earth materials and paving the way to the *desiderata* of property engineering.

There are several advantageous characteristics that this fully non-empirical LFDFT method possess and should be noted and remembered, besides the predictive capability, very important today for the vast number and kind of rare-earth based technological materials. The method can be applied to any lanthanide ions for general $4f^n$ – $4f^{n-1}5d^1$ transitions with different coordination symmetries. The LFDFT approach has other advantages against widespread semi-empirical and full *ab initio* method, not least the fact that it can be applied to bigger size systems in a relatively short computational time.

Acknowledgements

This work is supported by the Swiss National Science Foundation (SNF) and the Swiss State Secretariat for Innovation and Research. Support from the UEFISCDI Romania research grant PCE 14/2013 from the Romanian Ministry of Research is also acknowledged.

Notes and references

[a] *Department of Chemistry of the University of Fribourg (Switzerland), Chemin du Musée 9, 1700 Fribourg, Switzerland, Fax: +41 26 300 9738; Tel: +41 26 300 8700; E-mail: harry.ra@hotmail.com*

[b] *Laboratoire de physique de la matière et modélisation mathématique, LPQ3M, Université de Mascara, Algeria*

[c] *Faculty of Chemistry, Inorganic Chemistry Department, University of Bucharest, Dumbrava Rosie 23, Bucharest 0206462, Romania*

[d] *Institute of Physical Chemistry, Splaiul Independentei 202, Bucharest 060021, Romania; E-mail: cfanica@yahoo.com*

† Electronic Supplementary Information (ESI) available: [The whole range of the spectral energy obtained for the $CaF_2:Eu^{2+}$ and $SrCl_2:Eu^{2+}$ together with the direct comparison between the theoretical spectra and the excitation spectra in refs. [41] and [42]]. See DOI: 10.1039/b000000x/

1 H. Bethe, *Annalen der Physik*, 1929, **295**, 133.
2 J. H. Van Vleck, *J. Chem. Phys*., 1935, **3**, 807.
3 J. S. Griffith, The Theory of Transition Metal Ions, Cambridge University Press, Cambridge, 1961.
4 M. Gerloch, J. H. Harding and R. G. Woodley, *Struct. Bond*., 1981, **46**, 1.
5 B. N. Figgis and M. A. Hitchman, Ligand Field Theory and its Applications, Wiley-VCH, New York, 2000.
6 C. Schäffer and C. Jørgensen, *Mol. Phys.,* 1965, **9**, 401.
7 W. Urland, *Chem. Phys*., 1976, **14**, 393.
8 C. Daul, *Int. J. Quantum Chem*., 1994, **52**, 867.
9 C. Daul, E. J. Baerends and P. Vernooijs, Inorg. Chem., 1994, **33**, 3538.
10 M. Atanansov, C. A. Daul and C. Rauzy, *Struct. Bond*., 2004, **106**, 97.
11 L. Noodleman and J. G. Norman, *J. Chem. Phys*., 1979, **70**, 4903.
12 L. Noodleman, *J. Chem. Phys*., 1981, **74**, 5737.
13 M. Mitani, V. Mori, Y. Takano, D. Yamaki, Y. Yoshioka and K. Yamaguchi, *Chem. Phys*., 2000**, 113**, 4035.
14 A. Bencini and F. Totti, Int. *J. Quantum Chem*., 2005, **101**, 819.
15 F. Cimpoesu, B. Frescus, C. I. Oprea, H. Ramanantoanina, W. Urland and C. Daul, Mol. Phys., 2015, DOI: 10.1080/00268976.2015.1007107.
16 M. Atanasov, C. Rauzy, P. Baettig and C. Daul, *Int. J. Quantum Chem*., 2005, **102**, 119.
17 M. Atanasov, C. Daul, H. U. Gudel, T. A. Wesolowski and M. Zbiri, *Inorg. Chem*., 2005, **44**, 2954.
18 D. Reinen, M. Atanasov and W. Massa, *Z. Anorg. Allg. Chem*., 2006, **632**, 1375.
19 M. Atanasov, P. Comba and C. Daul, *Inorg. Chem*., 2008, **47**, 2449.
20 M. Gruden-Pavlovic, M. Peric, M. Zlatar and P. Garcia-Fernandez, *Chem. Sci*., 2014, **5**, 1453.
21 Z. D. Matovic, M. S. Jeremic, R. M. Jelic, M. Zlatar and I. Z. Jakovljevic, *Polyhedron*, 2013, **55**, 131.
22 G. Morrison, H. Ramanantoanina, W. Urland, M. D. Smith and H.-C. zur Loye, submitted to *Inorg. Chem*., 2015.
23 C. A. Daul, *J. Phys.: Conference Series*, 2013, **428**, 012023.
24 A. Borel, C. A. Daul and L. Helm, *Chem. Phys. Lett*., 2004, **383**, 584.
25 F. Senn, L. Helm, A. Borel and C. A. Daul, *Comptes Rendus Chimie*, 2012, **15**, 250.
26 M. Atanasov and C. A. Daul, *Chem. Phys. Lett*., 2003, **379**, 209.
27 M. Atanasov, P. Comba and C. Daul, *Inorg. Chem*., 2006, **110**, 13332.
28 I. Ciofini and C. Daul, *Coord. Chem. Rev*., 2003, **238-239**, 187.
29 M. Atanasov and C. A. Daul, *Comptes Rendus Chimie*, 2005, **8**, 1421.
30 M. Atanasov, E. J. Baerends, P. Bruyndonckx, C. Daul, C. Rauzy and M. Zbiri, *Chem. Phys. Lett*., 2004, **399**, 433.
31 F. Senn and C. A. Daul, J. *Molec. Struct.: TEOCHEM*, 2010, **954**, 105.

32 F. Senn, M. Zlatar, M. Gruden-Pavlovica and C. Daul, *Monatshefte für Chemie*, 2011, **142**, 593.
33 L. Petit, A. Borel, C. Daul, P. Maldivi, C. Adamo, *Inorg. Chem.*, 2006, **45**, 7382.
34 M. Atanasov and C. Daul, *CHIMIA International Journal for Chemistry*, 2005, **59**, 504.
35 H. Ramanantoanina, W. Urland, F. Cimpoesu and C. Daul, *Phys. Chem. Chem. Phys*., 2013, **15**, 13902.
36 H. Ramanantoanina, W. Urland, A. Garcia-Fuente, F. Cimpoesu and C. Daul, *Chem. Phys. Lett*., 2013, **588**, 260.
37 S. Nakamura and G. Fasol, The Blue Laser Diode, Springer, Berlin, 1997.
38 H. Ramanantoanina, W. Urland, A. Garcia-Fuente, F. Cimpoesu and C. Daul, *Phys. Chem. Chem. Phys*., 2014, **16**, 14625.
39 H. Ramanantoanina, W. Urland, B. Herden, F. Cimpoesu and C. Daul, *Phys. Chem. Chem. Phys*., 2015, **17**, 9116.
40 B. Herden, A. Garcia-Fuente, H. Ramanantoanina, T. Jüstel, C. Daul amd W. Urland, *Chem. Phys. Lett*., 2015, **620**, 29.
41 G. W. Burdick, A. Burdick, V. Deev, C.-K. Duan and M. F. Reid, *J. Lumin*., 2006, **118**, 205.
42 Z. Pan, L. Ning, B.-M. Cheng and P. A. Tanner, *Chem. Phys. Lett*., 2006, **428**, 78.
43 R. D. Cowan, *The theory of atomic structure and spectra*, University of California Press, Berkeley 1981.
44 H. Lueken, *Magnetochemie*, Teubner Studienbücher Chemie, Stuttgart 1999.
45 M. Gerloch. *Magnetism and ligand-field analysis*, Cambridge University Press, Cambridge 1983.
46 S. Hüfner, *Optical spectra of transparent rare earth compounds*, Academic Press, New Y ork 1978.
47 H. Ramanantoanina, W. Urland, F. Cimpoesu and C. Daul, *Phys. Chem. Chem. Phys*., 2014, **16**, 12282.
48 G. te Velde, F. M. Bickelhaupt, S. J. A. van Gisbergen, C. F. Guerra, E. J. Baerends, J. G. Snijders and T. Ziegler, *J. Comput. Chem*., 2001, **22**, 931.
49 C. F. Guerra, J. G. Snijders, G. te Velde and E. J. Baerends, *Theor. Chem. Acc*., 1998, **99**, 391.
50 E. J. Baerends, T. Ziegler, J. Autschbach, D. Bashford, A. Berces, F. M. Bickelhaupt, C. Bo, P. M. Boerrigter, L. Cavallo, D. P. Chong, L. Deng, R. M. Dickson, D. E. Ellis, M. van Faassen, L. Fan, T. H. Fischer, C. F. Guerra, A. Ghysels, A. Giammona, S. J. A. van Gisbergen, A. W. Götz, J. A. Groeneveld, O. V. Gritsenko, M. Grüning, S. Gusarov, F. E. Harris, P. van den Hoek, C. R. Jacob, H. Jacobsen, L. Jensen, J. W. Kaminski, G. van Kessel, F. Koostra, A. Kovalenko, M. V. Krykunov, E. van Lenthe, D. A. McCormack, A. Michalak, M. Mitoraj, J. Neugebauer, V. P. Nicu, L. Noodleman, V. P. Osinga, S. Patchkovskii, P. H. T. Philipsen, D. Post, C. C. Pye, W. Ravenek, J. I. Rodriguez, P. Ros, P. R. T. Shipper, G. Schreckenbach, J. S. Seldenthuis, M. Seth, J. G. Snijders, M. Sola, M. Swart, D. Swerhone, G. te Velde, P. Vernooijs, L. Versluis, L. Vissher, O. Visser, F. Wang, T. Wesolowski, E. M. van Wezenbeek, G. Wiesenekker, S. K. Wolff, T. K. Woo and A. L. Yarkolev, ADF2013.01, available at http://www.scm.com.
51 P. J. Stephens, F. J. Devlin, C. F. Chabalowski and M. J. Frisch, *J. Phys. Chem.*, 1994, **98**, 11623.
52 (a) G. Kresse and J. Hafner, *Phys. Rev. B: Condens. Matter Mater. Phys.*, 1993, **47**, 558; (b) G. Kresse and J. Furthmüller, *Phys. Rev. B: Condens. Matter Mater. Phys.*, 1996, **54**, 11169.
53 S. H. Vosko, L. Wilk and M. Nussair, *Canadian J. Phys*., 1980, **58**, 1200.
54 J. P. Perdew, K. Burke and M. Ernzerhof, *Phys. Rev. Lett*., 1996, **77**, 3865.
55 P. E. Blöchl, *Phys. Rev. B: Condens. Matter Mater. Phys.*, 1994, **50**, 17953.
56 G. Kresse and D. Joubert, *Phys. Rev. B: Condens. Matter Mater. Phys.*, 1999, **59**, 1758.
57 T. Ziegler, A. Rauk and E. J. Baerends, *Theor. Chim. Acta*, 1977, **43**, 261.
58 see also the two different manners devoted to the calculation of the Slater-Condon parameters in the two-open-shell $4f^2$ and $4f^15d^1$ configurations of Pr^{3+} in ref. [35] and [39].
59 P. Pyykkö and J. P. Desclaux, *Acc. Chem. Res*., 1979, **12**, 276.
60 K. S. Pitzer, *Acc. Chem. Res*., 1979, **12**, 271.
61 C. Clavaguera, J.-P. Dognon, P. Pyykkö, *Chem. Phys. Lett*., 2006, **429**, 8.
62 P. Pyykkö, *Chem. Rev.*, 1988, **88**, 563.
63 P. Pyykkö, *Chem. Rev.*, 2012, **112**, 371.
64 D. Cremer, W. Zou and M. Filatov, *WIREs Comput. Mol. Sci*., 2014, **4**:436.
65 E. van Lenthe, A. E. Ehlers and E. J. Baerends, *J. Chem. Phys*., 1999, **110**, 8943.
66 E. van Lenthe, E. J. Baerends and J. G. Snijders, *J. Chem. Phys*., 1993, **99**, 4597.
67 E. van Lenthe, E. J. Baerends and J. G. Snijders, *J. Chem. Phys*., 1993, **101**, 9783.
68 E. van Lenthe, J. G. Snijders and E. J. Baerends, *J. Chem. Phys*., 1996, **105**, 6505.
69 E. van Lenthe, R. van Leeuwen, E. J. Baerends and J. G. Snijders, *Int. J. Quantum Chem*., 1996, **57**, 281.
70 J. G. Snijders and E. J. Baerends, *Mol. Phys*., 1978, **36**, 1789.
71 J. G. Snijders, E. J. Baerends and P. Ros, *Mol. Phys*., 1979, **38**, 1909.
72 T. Ziegler, J. G. Snijders and E. J. Raerends, *J. Chem. Phys*., 1981, **74**, 1271.
73 T. Ziegler, V. Tschinke, E. J. Baerends, J. G. Snijders and W. Ravenek, *J. Phys. Chem*., 1989, **93**, 3050.
74 P. M. Boerrigter, M. A. Buijse and J. G. Snijders, *Chem. Phys*., 1988, **122**, 357.
75 R. D. Cowan and D. C. Griffin, *J. Opt. Soc. Am*., 1976, **66**, 1010.
76 A. Kramida, Y. Ralchenko, J. Reader and NIST ASD Team (2014). *NIST Atomic Spectra Database* (ver. 5.2), [Online]. Available: http://physics.nist.gov/asd [2015, April 21]. National Institute of Standards and Technology, Gaithersburg, MD.
77 C. W. Nielson and G. F. Koster, *Spectroscopic Coefficients for the p^n, d^n and f^n Configurations*, The MIT press Cambridge 1963.
78 R. E. Walstedt and L. R. Walker, *Phys. Rev. B*, 1974, **9**, 4857.
79 P. A. O'Day, J. J. Rehr, S. I. Zabinsky and G. E. Brown, *J. Am. Chem. Soc.*, 1994, **116**, 2938.
80 P. Ghina, A. Carollo, G. Flor, L. Malavasi and G. S. Peruga, *J. Phys. Chem. B*, 2005, **109**, 4365.
81 B. V. Padlyak, M. Grinberg, T. Lukasiewicz, J. Kisielewski and M. swirkowicz, *J. Alloys Comp*., 2003, **361**, 6.
82 D. N. Batchelder and R. O. Simmons, *J. Chem. Phys*., 1964, **41**, 2324.
83 H. Ott, *Zeitschrift für Kristallographie - Crystaline Materials*, 1926, **63**, 222.
84 C. K. Jørgensen, *Absorption Spectra and Chemical Bonding in Complexes*, Pergamon Press, Oxford 1962.
85 P. A. Tanner and Y. Y. Yeung, *J. Phys. Chem. A*, 2013, **117**, 10726.
86 D. L. Clark, J. C. Gordon, P. J. Hay and R. Poli, *Organometallics*, 2005, **24**, 5747
87 F. Cimpoesu, N. Dragoe, H. Ramanantoanina, W. Urland and C. Daul, *Phys. Chem. Chem. Phys*., 2014, **16**, 11337.
88 M. L. Neidig, D. L. Clark and R. L. Martin, *Coord. Chem. Rev*., 2013, **257**, 394.

